The Conserved N-Terminal Region of the Mitotic Checkpoint Protein BUBR1: A Putative TPR Motif of High Surface Activity

V. M. Bolanos-Garcia,* S. Beaufils,† A. Renault,† J. G. Grossmann,‡ S. Brewerton,* M. Lee,§ A. Venkitaraman,§ and T. L. Blundell*

*Department of Biochemistry, University of Cambridge, Cambridge, United Kingdom; †Groupe Matiere Condensee et Materiaux, Universite de Rennes, Campus de Beaulieu, Rennes, France; ‡Synchrotron Radiation Department, CCLRC Daresbury Laboratory, Warrington, United Kingdom; and §The Hutchison/MRC Research Centre, Cambridge, United Kingdom

ABSTRACT BUBR1, a key component of the mitotic spindle checkpoint, is a multidomain protein kinase that is activated in response to kinetochore tension. Although BUB1 and BUBR1 play an important role in cell division, very little is known about their structural characteristics. We show that the conserved N-terminal region of BUBR1, comprising residues 1–204, is a globular domain of high α-helical content ($\approx$60%), stable in the pH range 4–9 and probably organized as a tetratricopeptide motif repeat (TPR), most closely resembling residues 16–181 of protein phosphatase 5. Because the latter presents a continuous amphipathic groove and is regulated by binding certain fatty acids, we compared the properties of BUBR1(1–204) and TPR-PP5 (16–181) at air/water interfaces and found that both proteins exhibited a similar surface activity and formed stable, rigid monolayers. The deletion of a region that probably comprises several α-helices of BUBR1 indicates that long-range interactions are essential for the stability of the N-terminal domain. The presence of the putative TPR motif strongly suggests that the N-terminal domain of BUBR1 is involved in direct protein-protein interactions and/or protein-lipid interactions.

INTRODUCTION

Premature separation of sister chromatids leads to the loss or gain of chromosomes in daughter cells (aneuploidy), a prevalent form of genetic instability in human cancer (1). To avoid these disastrous consequences, eukaryotic cells have evolved a mechanism of control that ensures the high-fidelity transmission of genetic material in mitosis and meiosis (2). This mechanism delays the progression of mitosis until condensed chromosomes are properly positioned on the mitotic spindle. The mitotic checkpoint control monitors both the attachment of chromosomes to the mitotic spindle and the tension across the sister chromatids generated by microtubules (3). Even a single kinetochore is sufficient to prevent progression to anaphase, as demonstrated by classic laser irradiation and micromanipulation experiments (4,5).

The 120-kDa multidomain protein BUBR1 (also known as BUB1B) is expressed in most cell lines and is present during various stages of the cell cycle. It plays an essential role in mitotic checkpoint control by phosphorylation of critical cellular component(s) of the mitotic checkpoint pathway. However, as cells enter late S and G2 phases, BUBR1 levels increase significantly. BUBR1 binds to kinetochores (6), is able to inhibit Cdc20 in vitro (7) and is essential for the function of the protein Sgo1 (shugoshin), a protector of the centromeric cohesin Rec8 protein in fission yeast (8).

Human BUBR1 was first identified as an interacting protein of the kinetochore motor protein CENP-E (6) and also as a protein that contains regions homologous to yeast Mad3 and BUB1 (9). Mutations in the *hbub1* and *hbubr-1* genes have been detected in gastric cancer (10). Furthermore, the recent identification of truncating and missense mutations of BUBR1 in families with mosaic-variegated aneuploidy suggests that there is a causal link between aneuploidy and cancer development (11).

In contrast to BUB1, BUBR1 does not exhibit asymmetry in prometaphase cells: only when both kinetochores are attached do they come under tension, and then a reduction in the amount of BUBR1 at the kinetochore occurs simultaneously. Antibody injection experiments have shown that repression of BUBR1 compromises spindle checkpoint function (3). BUBR1 RNAi cultures did not accumulate mitotic cells on exposure to spindle toxins. However, prometaphase cells in BUBR1 RNAi cultures often appear abnormal with the chromosomes aligned along the length of the spindle rather than at the metaphase plate. Although these chromosomes appear to be attached to the spindle, the mean interkinetochore distance is reduced compared with control cells, consistent with a reduction in pulling forces. The conserved N-terminal region of BUBR1 exhibits a putative KEN box motif (12). This motif is present in Mad3-like proteins as a short N-terminal extension and it has been reported to act as a Cdh1-dependent anaphase-promoting complex (APC) recognition signal (13). A BUBR1/BUB3 complex efficiently inhibits the APC in a process that is Mad-2-independent (7). Interestingly, despite the conservation of the N-terminal domain of BUB1/BUBR1 proteins, the KEN motif is absent in BUB1. The implications of this difference for the function of BUB1 remain to be elucidated.

Submitted March 25, 2005, and accepted for publication June 22, 2005.

Address reprint requests to Victor M. Bolanos-Garcia, Dept. of Biochemistry, University of Cambridge, 80 Tennis Court Rd., Cambridge CB2 1GA, England. Tel.: 44-1223-766029; Fax: 44-1223-76602; E-mail: victor@cryst.bioc.cam.ac.uk.

0006-3495/05/10/2640/10 $2.00

doi: 10.1529/biophysj.105.063511

The tetratricopeptide motif repeat (TPR) was first identified in the cell cycle division proteins cdc16, cdc23, and cdc27 as a degenerate tandem repeat of 34 amino acid residues encoding an α-helix-turn-α-helix motif (14). Mutations within the TPR motifs of these proteins cause mitotic arrest at the metaphase-to-anaphase transition. TPRs have now been identified in a wide diversity of organisms, ranging from bacteria to humans. This motif, which is known to mediate protein-protein interactions, exists in proteins of diverse biological functions such as cell cycle regulation, neurogenesis, transcription control, mitochondrial and peroxisomal protein transport, Rac mediated activation of NADPH oxidase, protein kinase inhibition, and protein folding (15). In TPR-containing proteins, this repeat motif is often present in tandem arrays of 3–16 motifs, although individual TPR motifs or blocks of TPR motifs may be dispersed throughout the protein sequence.

The crystal structure of the TPR motif of protein phosphatase 5 residues 16–181 (TPR-PP5(16–181)) shows that this region contains three TPR motifs (16). Adjacent TPR motifs are packed together to form a regular series of antiparallel α-helices rotated relative to one another by a constant 24°. The uniform arrangement of neighboring α-helices gives rise to the formation of a right-handed superhelical structure that creates a regular, elongated amphipathic (i.e., one side hydrophobic and the other hydrophilic) groove. This topology also creates a continuous concave surface on one side with a contrasting convex surface on the other. The elongated amphipathic groove defined a novel mechanism for protein recognition and constitutes a suitable platform for target proteins of PP5 (16). The TPR motif mediates the interaction of PP5 with the mammalian cryptochromes CRY1 and CRY2 (17) and the single transmembrane atrial natriuretic peptide receptor (18). The TPR motif of PP5 also acts as the regulatory domain of the C-terminal phosphatase in a process that involves the direct interaction of the TPR motif with certain lipids such as arachidonic acid (19).

Langmuir monolayers at the air/water interphase have been thoroughly studied for a long time. However, advances have been achieved in recent years because of new experimental techniques such as ellipsometry, polarized fluorescence microscopy, and Brewster angle microscopy (BAM). These novel techniques, when applied to the analysis of proteins at interfaces have yielded relevant physicochemical information. For example, a series of experiments with protein films coupled to BAM demonstrated that the singularities in the surface pressure-area isotherms are due to phase changes, where each phase has a different molecular organization (20). Other studies have focused on the molecular orientation of tetra-α-helical heme proteins (αssα)2 (21) and the interfacial properties of lipid-binding proteins (22; reviewed in Bolanos-Garcia and Nunez-Miguel (23)).

We show that the N-terminal domain of BUBR1 is globular, predominantly α-helical, stable in a wide range of pH, and likely to contain the TPR motif. The latter suggestion is further supported by a series of comparative studies of this BUBR1 region and TPR-PP5 that include measurements of shear elastic constant and surface activity using Langmuir-Blodgett films coupled to BAM and null-ellipsometer. Taken together, our studies constitute the first report on the biophysical, biochemical, and structural characterization of the N-terminal domain of BUBR1.

MATERIAL AND METHODS

Materials

Vector pGEX4T-1, glutathione-sepharose resin, high-purity thrombin, and the chromatography columns XK 26, Superdex 75 Hiload 26/60, sepharose-glutathione fast flow and benzamidine fast flow were from Amersham Pharmacia (Uppsala, Sweden). Ni-NTA resin was from Qiagen (West Sussex, UK). Tablets of a cocktail of protease inhibitors were from Boehringer Mannheim (Roche Diagnostics, East Sussex, UK). All the BUBR1 protein constructs were expressed in *Escherichia coli* BL21 (DE3). TPR-PP5(16–181) was expressed in BL21 Codon plus. Both bacteria strains were from Stratagene (Cambridge, UK). Quartz cells for circular dichroism (CD) were from Hellma (Essex, UK). Benzamidine, imidazole, and all the salts used for preparing buffer solutions were from Sigma (St. Louis, MO). Buffer and protein solutions were prepared with ultrapure water (Nanopure-UV).

Methods

Cloning, expression, and purification of soluble constructs

The gene region encoding the N-terminal domain of human BUBR1(1–204) was extended using conventional polymerase chain reaction. The amplicon thus generated was cloned in frame downstream of the gst gene in the pGEX4T-1 vector in the BamHI and SalI cloning sites. The identity of the resulting vector, pGST-CD1, was confirmed by DNA sequencing. *E. coli* BL21 (DE3) cells were transformed with the plasmid pGST-CD1 and the protein BUBR1(1–204), expressed as follows: when the optical density at 600 nm of bacterial cultures grown in 2xTY broth was 0.6–0.7, cells were induced with 0.1 mM isopropyl-β-D-thiogalactopyranoside. Cells were harvested 4–5 h after induction. The cell pellet was washed with TBS buffer (0.04 M Tris, 0.2 M NaCl, pH 7.4), centrifuged 20 min at 8000 rpm and stored at −70°C until use. Frozen cell pellets were thawed on ice and resuspended in TBS buffer containing a cocktail of protease inhibitors. Cells were lysed in a French press at 1200 psi (SIM Aminco, Darmstadt, Germany). After centrifugation at 20,000 rpm for 1 h at 4°C, the soluble fraction was loaded onto an XK 26 column packed with glutathione-sepharose resin previously equilibrated in the same buffer solution. After washing with ~20 volumes of TBS, 1 unit protease was used to digest 1 mg of recombinant GST-BUBR1 fusion. Thrombin and free GST-tag were removed using a benzamidine fast flow column and a sepharose-glutathione column, respectively. A protocol similar to that described above was used for the cloning, expression, and purification of other GST fusions, including BUBR1(36–204), (1–184), (1–192), (1–147), (210–340), (221–320), and (230–340).

TPR-PP5(16–181) containing a 6x-histidine tag at the N-terminal region was expressed in *E. coli* BL21 Codon plus and purified by Ni-NTA affinity chromatography according to conventional protocols. The identity of each recombinant protein was confirmed by MALDI-TOF and N-terminal sequencing at the PNAC facility (Department of Biochemistry, University of Cambridge, Cambridge, UK). The N-terminal sequence analysis was carried out according to the Edman degradation technique.

In silico analysis

The hydrophobic moment (μH) (24) was calculated using the program (Hmoment) (available at http://bioweb.pasteur.fr/seqanal/interfaces/

hmoment.html). The average hydrophobic moment (μH_{avg}) of the amphipathic α-helices of BUBR1(1–204) was estimated according to Eq. 1:

$$\mu H_{avg} = \sum_{n=1}(1/N[[\sum_{n=1} Hn \sin(\delta n)]^2 + [\sum_{n=1} Hn \cos(\delta n)]^2]^{1/2}), \quad (1)$$

where δ corresponds to the angle formed between amino acid lateral chains of two adjacent residues with respect to the plane of the α-helix (for an ideal α-helix, $\delta = 100°$); $N =$ the number of residues in that α-helix, and Hn is the numerical hydrophobicity of the nth residue. Hn values are related to the free energy of transfer of the amino acids from the inside to the surface of a globular protein.

The α-helix consensus regions of BUBR1(1–204) were predicted using the MetaPredict Protein server (http://cubic.bioc.columbia.edu/predictprotein) and the suite of programmes described below.

A new implementation of the FUGUE program FugueRep (25,26) was used to search for the TPR repeat motif in the BUBR1 sequence. Structural profiles were created from the coordinates of each known TPR repeat protein deposited in the Protein Data Bank. These were protein phosphatase 5 (1a17), neutrophil cytosol factor 2 (1e96), hop chaperone (1elr, 1elw), human pex5 (1fch), and bovine cyclophilin 40 (1ihg). The coordinates of each Protein Data Bank entry were split into a number of files containing single repeat units. These were then structurally aligned using COMPARER (27) and structural profiles representing a single repeat motif were built from the alignment using Melody (25). Each profile was then used to search the BUBR1 sequence using the FUGUE algorithm. Where FUGUE was able to align the profile with a region of the sequence, the hit was noted, the region of the sequence masked, and the profile search repeated until no more hits were found. As FUGUE scores alignments based on environment specific substitution tables and structure-dependent gap penalties, the FugueRep method seems to be more sensitive for the detection of structural repeats than other sequence-based methods (26).

Circular dichroism

Far-ultraviolet (UV) circular dichroism spectra of recombinant, BUBR1 (1–204) were recorded on a Jasco J-720 spectropolarimeter (Jasco, Tokyo, Japan) previously calibrated with camphorosulfonic acid and equipped with a temperature control unit (JASCO PTC-348). Spectra were recorded in a 0.1-cm quartz cell, using an average time of 0.3 s and a step size of 0.5 nm at 20°C. The global α-helix content was calculated using the program CDPro (28) and from the molar residue ellipticity at 222 nm, essentially using the method previously reported (29). The signal dependence on protein concentration was calculated using several samples, with concentrations ranging between 50 μg/ml and 200 μg/ml (i.e., 2–8 μM) in 0.05 M sodium phosphate buffer, pH 7. For studies on protein stability as a function of pH, protein solutions were prepared in 0.05 M sodium acetate, pH 4 and 5; 0.050 M sodium phosphate buffer, pH 6, 7, and 8, and 0.05 M sodium borate, pH 9. In all experiments, spectra were recorded with a 1-nm bandwidth, 0.5-nm increment, and 20-s accumulation time, and were averaged over seven scans. After subtraction of the buffer baseline, the CD data were normalized and reported as molar residue ellipticity. The concentration of protein solutions was determined from UV absorbance measurements based on the molar absorption coefficient value (ε).

Small angle x-ray scattering

Data were collected at Station 2.1, Synchrotron Radiation Source, Daresbury Laboratory, using a two-dimensional multiwire proportional counter at sample-to-detector distances of 1.25 and 4.25 m. Data from matching buffers (0.050 M Tris-HCl, 0.15 M NaCl, and 0.001 M DTT, pH 7) were collected and subtracted from the protein profiles. BUBR1(1–204) solutions at concentrations ranging from 4 to 10 mg/ml ($\approx$160–400 μM) were analyzed at 20°C. The radius of gyration, R_g, the maximum particle dimension, D_{max}, and intraparticle distance distribution function, $[p(r)]$ were calculated from the scattering data using the indirect Fourier transform method program Gnom (30).

Ellipsometry, surface pressure measurements, and Brewster angle microscopy

Monolayers were prepared on a circular trough ($S = 20$ cm^2) and the surface pressure was measured with a sensor (Nima Technology, Cambridge, UK) using a Wilhelmy plate. The ellipsometric measurements were carried out with a house-made ellipsometer (31) operated with He-Ne laser ($\lambda = 632.8$ nm, Melles Griot, Carlsbad, CA) polarized with a Glan-Thompson polarizer (Melles Griot). The incidence angle of the light on the surface was 1° away from the Brewster angle. After reflection on the water surface, the laser light passed through a $\lambda/4$ retardation plate, a Glan-Thompson analyzer, and a photomultiplier. Through a computer-controlled feedback loop, the analyzer automatically rotated toward the extinction position. In this ''null ellipsometer'' configuration (32) the analyzer angle, multiplied by 2, yielded the value of the ellipsometric angle (Δ), i.e., the phase difference between parallel and perpendicular polarization of the reflected light. The laser beam probed a surface of 1 mm^2 and a depth in the order of 1 μm. The ellipsometric angle, Δ, is proportional to the quantity of protein adsorbed at the interface in the case of a monolayer. Hence, the variation of the ellipsometric angle is a relevant probe for changes occurring at the interface. Using the measured ellipsometric angle, Δ, and estimating the refractive index increment of the protein to 0.2 ml/g, the surface concentration, Γ, of adsorbed protein was calculated using the relationship between Δ and Γ reported by De Feijter and Benjamins (33). Initial values of the ellipsometric angle (Δ_0) and surface tension of pure buffer solutions were recorded on the subphase for at least half an hour. These values have been subtracted from all data presented below. Values of Δ and surface pressure (π) were stable and recorded every 4 s with a precision of $\pm$0.5 and $\pm$0.5 mN/m, respectively. Protein concentration used for ellipsometry, surface pressure measurements, and BAM observations was in the range 1–80 μg/ml in phosphate buffer (0.02 M sodium phosphate, pH 7).

Shear elastic constant

The principles and implementation of our experimental setup for the measurement of the lateral rigidity of monolayers and the procedure for data analysis have been extensively described before (34,35). Briefly, at the center of a 48-mm-diameter Teflon trough, a 10-mm-diameter paraffin-coated aluminum disc floats at the air/water interface, in contact with the monolayer, whose rigidity is measured. The subphase is 5 mm deep. The float carries a small magnet and is kept centered by a permanent magnetic field, $B_0 = 6 \times 10^{-5}$ T, parallel to the Earth's field and created by a small solenoid located just above the float. Sensitive angular detection of the float rotation is achieved by using a mirror fixed on the magnet to reflect a laser beam onto a differential photodiode. A sinusoidal torque excitation is applied to the float in the 0.01–100 Hz frequency range by an oscillating field perpendicular to the permanent solenoid field. The latter field acts as a restoring torque equivalent to a monolayer with a rigidity of 0.16 mN/m. This number set the sensitivity limit of the rheometer. The device behaves like a simple harmonic oscillator. The resistance that the monolayer opposes to the rotation of the float is directly measured. An important advantage of this setup is the absence of physical link between the outside and the float torsion (i.e., no torsion wire). This allows high sensitivities such that the applied deformation is very small, below $u_{xy} \sim 10^{-7}$ where u_{xy} corresponds to the deformation tensor (34). The amplitude and phase of the angular response, which reflects the rotational strain of the monolayer, is measured. The shear elastic constant (μ), which is expressed in mN/m, is measured at 5 Hz. Initial time points of all graphs ($t = 0$) correspond to the first possible measurements once the magnetic float is centered and stable, i.e., a few minutes after mixing.

For the experimental procedure, the amplitude and phase of the mechanical response of the pure subphase was first analyzed in the frequency range 0.01–100 Hz. Then the protein solution was directly dispensed in the trough and the mechanical response of the layer formed at the interface recorded at the fixed frequency of 5 Hz up to the end of kinetic. At this step, a complete measurement between 0.01 Hz and 100 Hz was performed again. Rigidity measurements were carried out in parallel to ellipsometry. All the experiments were performed at 18°C.

RESULTS

Fold recognition of the BUBR1(1–204) domain

The FugueRep (26) analysis of BUBR1 revealed two regions of the sequence where each of the TPR structural profiles consistently indicates the presence of a TPR motif in the human BUBR1 sequence and its homologs in mouse, rat, chicken, and frog. These regions correspond to residues 149–189 and residues 421–458 in the human sequence. For the first predicted repeat region the highest Z-score obtained was 5.56 and the lowest was 2.53. FUGUE Z-scores $\geq$6 are reported to indicate ''certain'' hits, $\geq$4 indicate ''likely'' hits, $\geq$3.5 indicate ''marginal'' hits, $\geq$2 indicate ''guess'' hits and $<$2 are uncertain (25). The average Z-scores (number of standard deviations above the mean score obtained by chance) were 3.67 and 1.97, respectively. Thus, the first predicted TPR motif is within range for marginal hits and the second is uncertain. However, many of the individual scores for hits in this region are in the likely range. The first repeat region predicted by FugueRep (residues 149–189) is in agreement with the predictions of REP, PROSITE, and SMART motif detection programs. Moreover, as shown in Fig. 1, this region shows good conservation of some of the residues previously reported for this structural unit (36). A lower conservation was observed in the other hit region (421–458) (data not shown).

Disorder prediction programs DISEMBL and GlobPlot were used to assess the presence of disordered regions in this protein. When using the loops/coils definition, DISEMBL predicts that many of the residues in the region 234–379 correspond to unstructured coil between secondary structures. Likewise, the assignment of globular domains using the Russell/Linding definition in GlobPlot also suggests that the region 260–387 and other shorter regions predominantly correspond to random coils with a marginal content of α-helical structure. In agreement with these predictions, we have observed a poor stability of several GST-BUBR1 fusions expressed in *E. coli*, including protein constructs encompassing the residues 210–340, 221–320 and 230–450.

FIGURE 1 Alignment of BUBR1 homologs. The human homolog corresponds to residues 149–189. This region is the strongest hit from the FugueRep analysis and is predicted to be a TPR motif. The canonical residues that have been reported for the TPR motif at those specific positions are shown in bold above the aligned sequences.

BUBR1(1–204) is a stable, α-helical, globular domain

The far-UV CD spectra of BUBR1(1–204) (Fig. 2 *A*) are consistent with an α-helix content of 62%, stable in the pH range 6 to 9 in the concentration range 50–200 μg/ml (2–8 μM). In contrast, at pH $<$3 a much lower content of α-helical structure and the predominance of disorder structure were noticed (Fig. 2 *A*), which reflect the instability of this protein domain at this extreme condition. Analytical gel filtration chromatography and solution x-ray scattering studies of BUBR1(1–204) at higher concentration (i.e., in the order 10–15 mg/ml, $\approx$400–600 μM) demonstrated that this globular and compact domain is predominantly dimeric, although a small amount of tetramer was also detected (manuscript in preparation). The estimated gyration radii of BUBR1(1–204) in the same concentration range is 32 Å, which is close to that estimated from the crystal structure of TPR-PP5(16–181) ($\approx$33 Å), where the protein was found to form dimers (16). Heat unfolding of BUBR1(1–204) monitored by CD spectroscopy showed a reversible denaturation profile, which was similar to that of peptides of high α-helical content (V. M. Bolanos-Garcia, manuscript in preparation).

BUBR1(1–204) is predicted to be a surface-active domain

Some of the nine predicted α-helices of BUBR1(1–204) seem to be of an amphipathic nature. Because the affinity of this class of α-helices for water/air interfaces is importantly

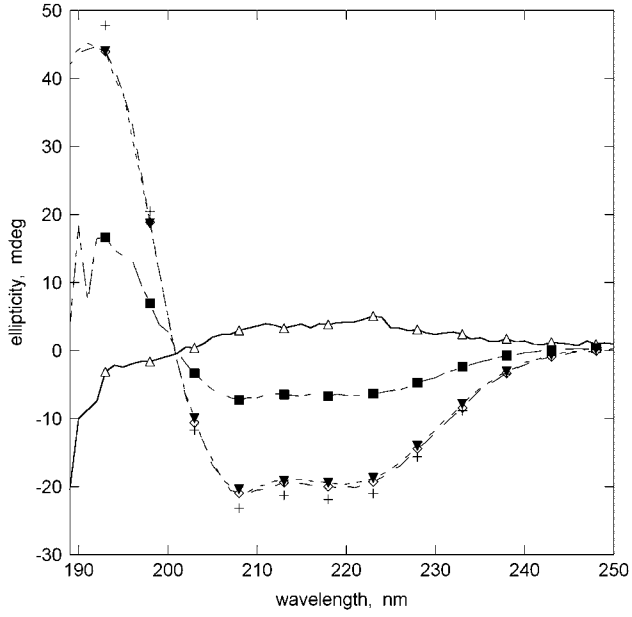

FIGURE 2 Far-UV spectra of human BUBR1(1–204) at pH 2 (△), 4 (■), 6 (◇), 8 (▼), and 9 (+).

influenced by the magnitude of the hydrophobic moment (μH), this parameter was estimated for each of the predicted helices of this domain. These μH values were as follows: helix 1 (10–28), 0.24; helix 2 (38–45), 0.11; helix 3 (53–68), 0.37; helix 4 (76–88), 0.33; helix 5 (98–110), 0.46; helix 6 (119–131), 0.50; helix 7 (135–144), 0.19; helix 8 (148–180), 0.36; and helix 9 (186–204), 0.34 kcal/mol. The average hydrophobic moment (μH_{avg}) was 0.32 kcal/mol per residue, which is similar to that observed in surface-active proteins such as apoA-II (μH_{avg} = 0.41 kcal/mol per residue) and apoC-III (μH_{avg} = 0.32 kcal/mol per residue) (37) and higher than less surface-active proteins such as lysozyme (μH_{avg} = 0.18 kcal/mol per residue) or ribonuclease A (μH_{avg} = 0.13 kcal/mol per residue) (38). The product $\mu H_{avg} \times F$, where F corresponds to the fraction of α-helix structure, is a good estimate of the theoretical surface pressure of α-helical proteins (39). As shown in Fig. 3, the magnitude of this product suggests that BUBR1(1–204) and TPR-PP5(16–181) exhibit surface activity at water/air interfaces.

BUBR1(1–204) forms a homogeneous, stable, rigid film at the air-water interface

BUBR1(1–204) was directly dispensed in the trough at a final concentration of 30 μg/ml (1.2 μM). The ellipsometric angle Δ at equilibrium (20 $\pm$ 1°), which is proportional to the quantity of protein adsorbed at the interface, as well as the maximum surface pressure (17 mN/m), confirmed that this domain is highly surface-active and able to form stable monolayers (Fig. 4). After 8 h, the surface concentration remains constant at 3.8 mg/m^2. As shown in Table 1, the maximum surface pressure of BUBR1(1–204) is comparable to that of other surface-active, α-helical proteins of similar size and oligomerization state at low concentration, such as exchangeable apolipoproteins C-I and A-I. TPR-PP5(16–181) and BUBR1(1–204) exhibit a higher surface pressure than other reported proteins such as lysozyme and human serum albumin (31% and 68% α-helix, respectively), at a similar surface concentration (38).

Adsorbed surface concentration and surface pressure of BUBR1(1–204) and TPR-PP5(16–181) have also been recorded at low bulk concentration (C_b= 1 μg/ml; i.e.,

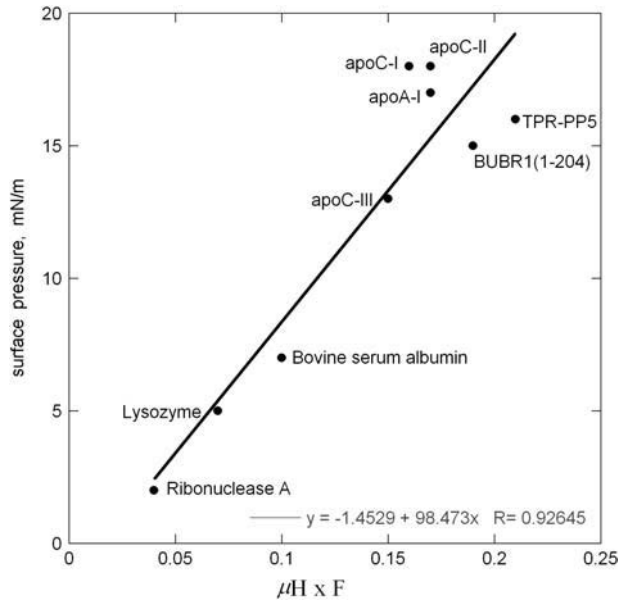

FIGURE 3 Theoretical surface pressure variation as a function of the product $\mu H_{avg} \times F$. TPR-PP5(16–181) and BUBR1(1–204) are predicted to be surface-active proteins.

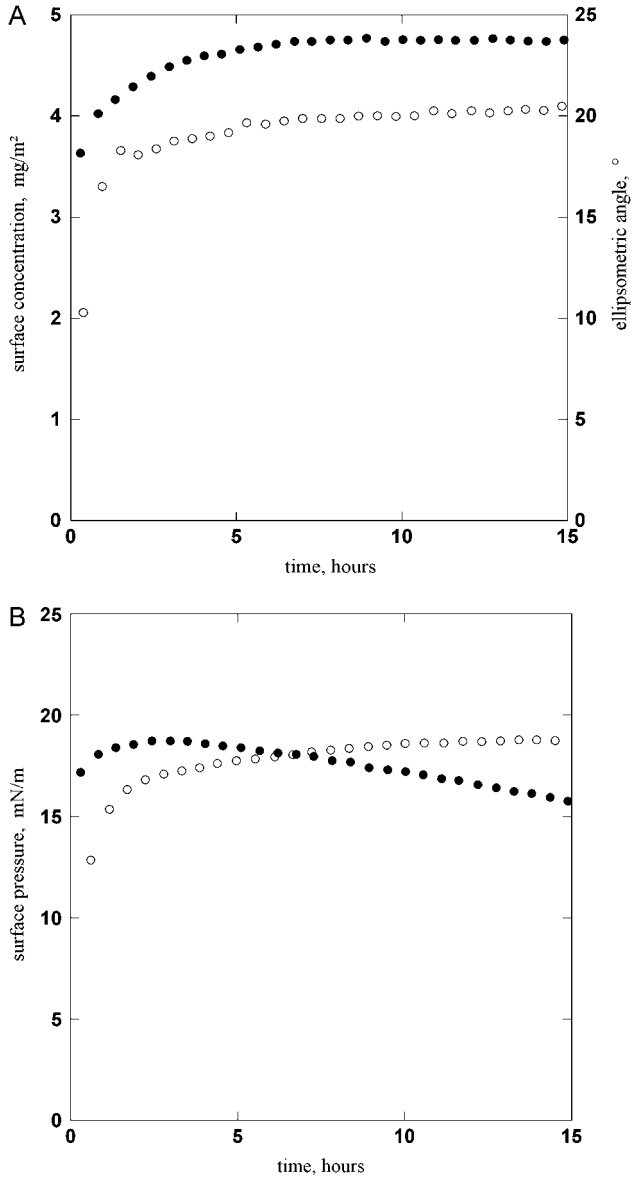

FIGURE 4 (*A*) Ellipsometric measurements of BUBR1(1–204) (○) and TPR-PP5(16–181) (●) at 30 μg/ml (i.e., 1.2 μM and 1.5 μM, respectively), pH 7. (*B*) Surface pressure measurements of BUBR1(1–204) (○) and TPR-PP5 (16–181) (●) at 30 μg/ml, pH 7.

TABLE 1 Comparison of the maximal surface pressure of several surface-active proteins recorded in the steady state

Protein	π (mN/m) in the steady state
Apolipoprotein C-I*	21
Apolipoprotein A-I*	19
BUBR1(1–204), pH 7	18
BUBR1(1–204), pH 2	28
BUBR1(36–204)	18
TPR-PP5(16–181)	18

*Values taken from V. M. Bolanos-Garcia, unpublished data.

40 nM and 50 nM, respectively). At this protein concentration, the first adsorption events could be recorded, which in turn allowed several parameters relevant to surface activity to be extracted. Two of these parameters were obtained from the plot of Γ versus π (Fig. 5). Here, Γ_0 is the surface concentration at which the surface pressure becomes different from zero. θ was extracted from the slope of the Γ-π curve and corresponds to the increase of surface pressure relative to the increase of surface concentration (40). Furthermore, in the first steps of adsorption of BUBR1(1–204) at this low bulk concentration, the transport of protein molecules from the subphase to the interface is assumed to be a diffusion-controlled process. Therefore, the surface concentration Γ follows the relation of Ward and Tordai (41), which is shown in Eq. 2:

$$\Gamma = 2C_b(Dt/3.1416)^{1/2}. \quad (2)$$

The initial part of the Γ-$t^{1/2}$ plot shows a linear correlation, making possible the calculation of the diffusion coefficient, Dt. For BUBR1(1–204), $Dt = 4.8\ 10^{-10}$ m^2/s, $\Gamma_0 = 1.1$ mg/m^2, and $\theta = 10$ mN $\times$ m/mg. The value of the diffusion coefficient is quite comparable to that of globular proteins of a similar size (33). Because Γ_0 is slightly higher and θ rather lower than the values reported for many other surface-active proteins (40), it seems that BUBR1(1–204) does not belong to the group of extremely surface-active proteins.

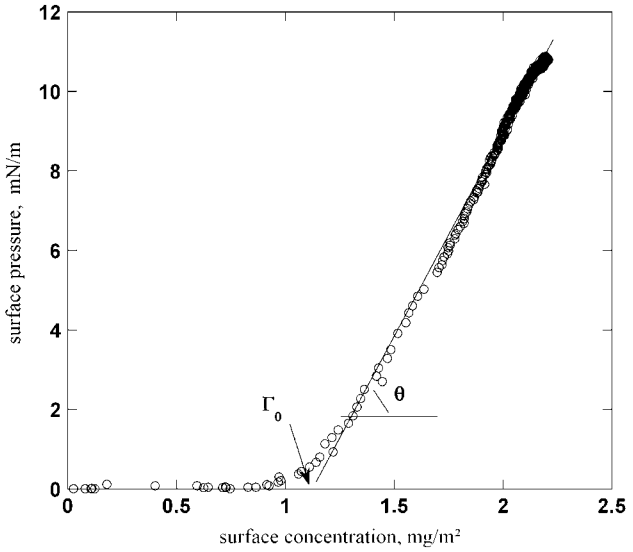

FIGURE 5 Surface pressure, π, versus surface concentration, Γ, calculated from ellipsometric and surface pressure measurements of BUBR1(1–204) at 1 μg/ml (40 nM), pH 7. θ corresponds to the slope $d\pi/d\Gamma$ and Γ_0 is the surface concentration at which the surface pressure becomes different from zero.

Effect of pH on the adsorption of BUBR1(1–204)

Because the CD analysis described previously showed that BUBR1(1–204) undergoes unfolding at pH 2 but remains folded at pH 7, these two pH conditions were selected for investigating the effect of the pH of the subphase on the properties of this domain at the air/water interface. As shown in Fig. 6, at pH 2 initial adsorption occurs rapidly and the maximal surface pressure reaches a steady-state condition after 30 min, which is much shorter than the time required to reach the same condition at pH 7 (i.e., ~8 h). Interestingly, a similar rapid migration from the bulk toward the interface has been observed in several well characterized surface-active lipid binding proteins of high α-helical content under similar experimental conditions (V. M. Bolanos-Garcia, S. Beaufils, and A. Renault, unpublished). The maximal surface pressure of BUBR1(1–204) at pH 2 is 28 mN/m, which is much higher than that measured at pH 7 (18 mN/m). In contrast, the maximal surface concentration of BUBR1 (1–204) at pH 2 is of the same order of magnitude as that at pH 7 (4.22 and 3.54 mg/m^2 $\pm$0.5 mN/m, respectively). Moreover, as Fig. 7 shows, the formation of a rigid monolayer occurs more rapidly at pH 2 than at pH 7: μ reaches a maximal value after 4 h and remains stable for at least 14 h.

Helix 1 is important for protein stability

Although the deletion mutant BUBR1(36–204) was overexpressed in *E. coli* as a soluble protein, it shows a higher content of disordered structure and a lower percentage of α-helix than BUBR1(1–204) as estimated by circular dichroism. In addition, BUBR1(36–204) was prone to form protein aggregates in aqueous solution, as detected by gel permeation chromatography and small angle x-ray scattering (data not shown). Consequently, a thermal stability analysis on BUBR1 (36–204) could not be carried out due to the poor reproducibility of independent thermal denaturation curves. However, this deletion mutant was studied in monolayers to evaluate the effect of deleting helix 1, which contains the putative KEN box motif, on the interfacial properties of BUBR1. BAM observations of BUBR1(1–204) and BUBR1 (36–204) are shown in Fig. 8. BUBR1(36–204) exhibits a similar surface pressure in the steady state as that of BUBR1 (1–204) (i.e., 18 mN/m). However, BAM observations showed that BUB1(36–204) exhibits a dramatic change in the refractive index at the interface compared with that of BUBR1 (1–204). In agreement with BAM observations, ellipsometry shows that BUBR1(36–204) forms a very disturbed layer, as Δ steadily increased for at least 15 h, the time frame during which the ellipsometric measurements were recorded.

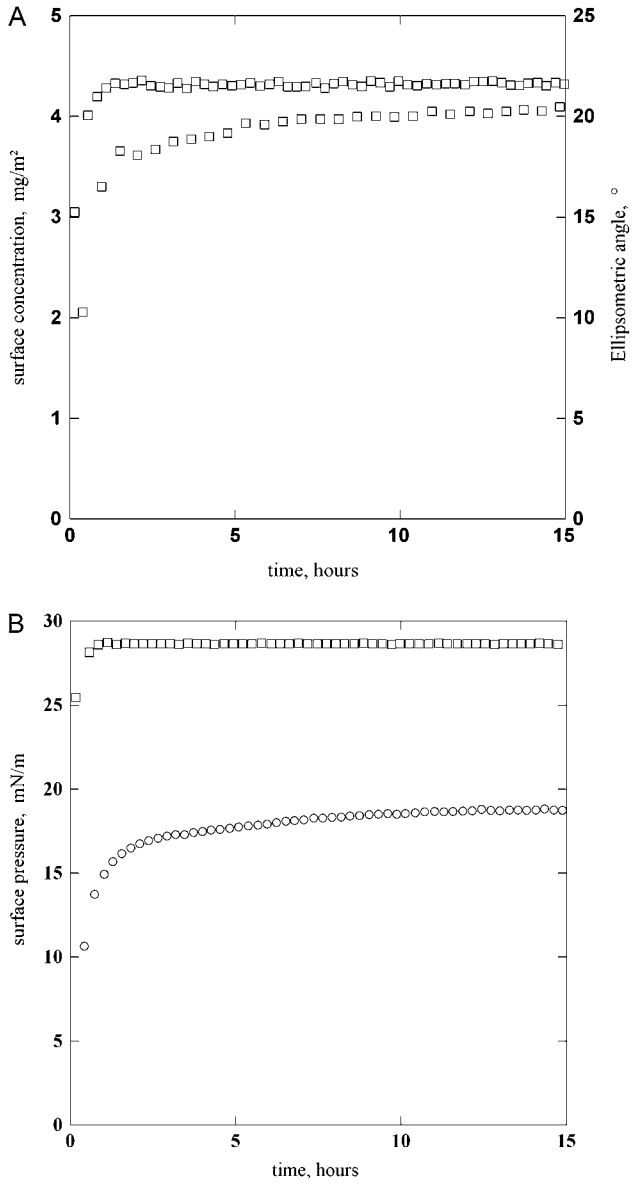

FIGURE 6 (*A*) Ellipsometric measurements of BUBR1(1–204) at pH 2 (□) and pH 7 (○). (*B*) Surface pressure of BUBR1(1–204) at pH 2 (□) and pH 7 (○).

The TPR motif of PP5(16–181) is also surface-active

TPR-PP5(16–181) also exhibits surface activity at interfaces, with similar adsorption kinetics to that of BUBR1(1–204), as shown in Fig. 4. In contrast to BUBR1(1–204), which remained adsorbed at the interface for at least 18 h, TPR-PP5(16–181) showed a relaxation of the surface pressure as early as 2 h after the experiment started. However, the surface concentration of this protein domain remained constant from 5 h after the beginning of kinetic. The maximal surface pressure reached was 18 mN/m, which is very similar to that of BUBR1(1–204) at pH 7. The final surface concentration is 4.7 mg/m^2, suggesting that TPR-PP5(16–181) is not forming

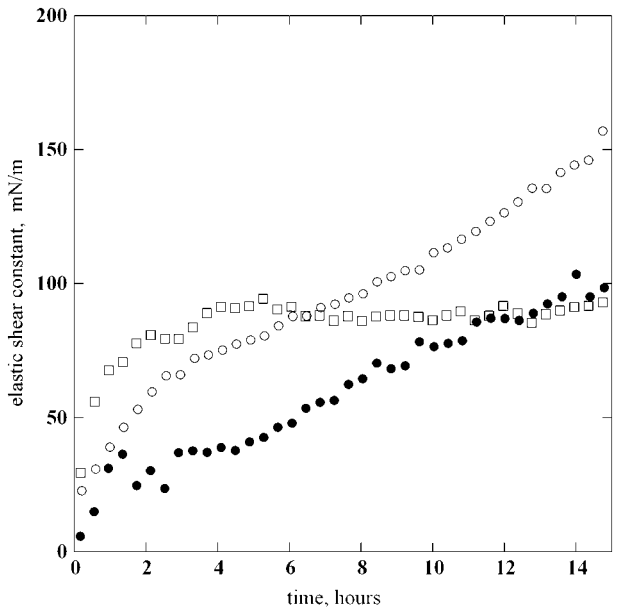

FIGURE 7 Rheology measurements of BUBR1(1–204) (○) and TPR-PP5(16–181) (●) at 30 μg/ml (i.e., 1.2 μM and 1.5 μM, respectively), pH 7, and of BUBR1(1–204) at 30 μg/ml, pH 2 (□). The graph shows the shear elastic constant, μ, versus time measured at the fixed frequency of 5 Hz, during protein adsorption at the interface.

protein multilayers. Thus, both proteins exhibit a similar surface activity and are able to form monolayers under identical experimental conditions.

To explore further the properties of the TPR-PP5(16–181) motif versus those of BUBR1(1–204), surface rheology measurements were carried out at pH 7 and pH 2. As shown in Fig. 7, rheology measurements suggest that monolayers of TPR-PP5(16–181) at pH 7 are comparatively less rigid than those of BUBR1(1–204) at the same pH value. Much less rigid TPR-PP5(16–181) monolayers were observed at pH 2 (μ in the steady state = 34 mN/m) compared with those at pH 7 (data not shown).

DISCUSSION

Our in silico analysis revealed two regions of BUBR1 in the human, mouse, rat, chicken, and frog homologs that might exhibit the TPR motif. These regions encompass residues 149–189 and 421–458 in the human sequence. However, the characteristic low residue conservation of TPR motifs makes it difficult to identify more distantly related TPR motif repeats. The TPR motif present in the N-terminal domain of BUBR1 seems to correspond to a single repeat, which is found less often than triple or higher order repeats in humans and other higher species (42). Interestingly, other proteins containing a single TPR motif unit in the N-terminal region include cdc16, cdc23, and cdc27, which play important roles in mitosis. However, the presence of more TPR units cannot be ruled out as individual hits scored in the likely range. We

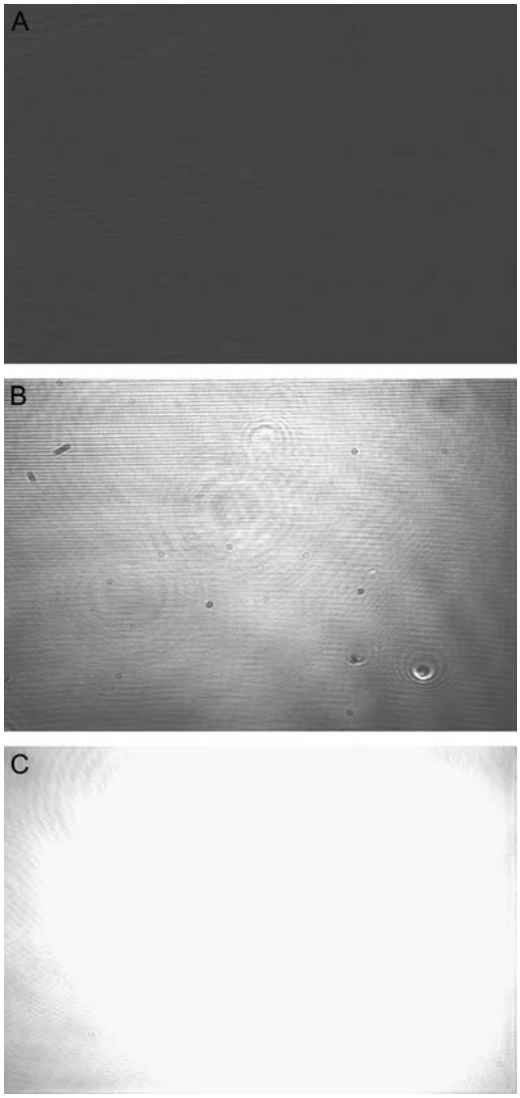

FIGURE 8 (*A*) BAM image (scale 300 μm $\times$ 500 μm) of pure buffer solution at zero time. (*B*) BAM image of BUBR1(1–204) at a concentration of 30 μg/ml (1.2 μM) adsorbed at 20°C, pH 7, at $t = 14$ h. (*C*) BAM image of BUBR1(36–204) obtained under conditions identical to those of BUBR1(1–204).

conclude from this analysis that the N-terminal domain of BUBR1 contains a divergent TPR motif repeat.

Because TPR-PP5 was the top hit of the structural profiles detected by FugueRep, we included in our study a series of comparative analyses between this motif and the N-terminal region of BUBR1. Due to the fact that the crystal structure of the TPR motif of PP5 shows the presence of a continuous amphipathic groove (16) and that this motif is able to bind certain fatty acids (19), the adsorption of TPR-PP5(16–181) and BUBR1(1–204) at air/water interfaces was investigated. The presence of a continuous amphipathic groove is not a unique feature of TPR-PP5, as it is also observed in the crystal structure of other TPR motifs, including that of Hop, cyclophilin 40, and Nlp1 (43–45). Thus, we postulate that TPR motifs are generally surface-active. However, whether the high surface activity is relevant for protein function will have to be established in each individual case.

TPR-PP5(16–181) and BUBR1(1–204) are predicted to be surface-active according to the product $\mu H_{avg} \times F$. The predicted surface-pressure values of BUBR1(1–204) and TPR-PP5(16–181) were in good agreement with those determined experimentally. Thus, the product $\mu H_{avg} \times F$ provides a good estimation of the relative surface activity of α-helical proteins containing amphipathic α-helices.

We observed a faster migration of TPR-PP5(16–181) toward the interface in comparison with BUBR1(1–204) at a similar concentration, which suggests the former exhibits a higher hydrophobicity. Because the surface concentration of TPR-PP5(16–181) remains constant, the decrease in surface pressure does not seem to be due to desorption events. Instead, molecular rearrangements may account for the adsorption dynamics of TPR-PP5(16–181).

The deletion mutant BUBR1(36–104) was prone to form aggregates and multilayers. The comparatively high surface pressure of BUBR1(36–204) at the similar surface concentration $\leq$4 mg/m^2 (the maximal surface concentration achieved by both BUBR1 constructs), strongly suggests that BUBR1 (36–204) undergoes dramatic conformational changes upon adsorption, including unfolding. As BUBR1(36–204) exhibited a surface pressure in the steady state similar to BUBR1 (1–204), we conclude that residues 36–204 are sufficient to confer surface activity on this domain. Helix 1(10–28) exhibits a low amphiphilicity (μH = 0.24 kcal/mol) and barely contributes to the global affinity of this protein domain for the interface. However, helix 1 (residues 10–28), which contains the KEN motif, confers stability to the N-terminal domain of BUBR1 in aqueous solutions and at interfaces. If the structural stabilization of this domain is a requirement for the function in vivo of the KEN motif as a Cdh1-dependent anaphase-promoting complex recognition signal, it is an aspect that requires further investigation.

The pH of the subphase has a significant influence on the properties of BUBR1(1–204) at the air/water interface, as changes in the pH of the solution affect the lateral interaction between protein molecules. If BUBR1(1–204) was unfolded at pH 7, a similar maximum surface pressure to that observed at pH 2 would be expected. In contrast, despite the similar surface concentration, the maximum pressure at pH 2 is much higher than that at pH 7, suggesting that BUBR1(1–204) is at least partially folded during early adsorption events. Because the transition from longways-on to sideways-on adsorption (tilting) is driven by packing requirements (46), a plausible explanation for the increase in the amount of protein adsorbed at pH 2 with respect to that at pH 7 is that when more molecules approach the surface, they might push together some of the previously adsorbed molecules, so that the layer becomes more compact and presents smaller loops and tails.

The rotation coupling between the float and the contacting monolayer was satisfactory because we measured the sur-

face shear elasticity using a device that introduces very small excitation strains (from 10^{-3} down to 10^{-6}) to our system. We have previously shown that pure shear elastic response exhibits a linear stress-strain relationship over this range (34) and that the small strains do not create plastic deformations on fragile surface objects (35).

Surface rheology of BUBR1(1–204) and TPR-PP5 (16–181) at pH 7 indicate that both proteins exhibit a similar adsorption kinetic. In comparison with BUBR1(1–204), TPR-PP5(16–181) forms less rigid monolayers, which is consistent with the notion that this motif undergoes molecular rearrangements at the interface. Nevertheless, the rigidity of TPR-PP5(16–181) at pH 7 is relatively high, strongly suggesting that this motif presents extensive medium-range and long-range interactions. Extensive medium- and long-range interactions are the ones most frequently observed in α-helical proteins compared with other structural classes, including all-β, $\alpha + \beta$ and α/β (47). Indeed, the mediation of long-range interactions is one important functional characteristic of TPR motifs (36). Thus, the stabilization of TPR motifs by medium- and long-range interactions provides an explanation of the poor stability in solution of other BUBR1 constructs where several α-helices were deleted, including that of α-helix 9 (residues 185–204 and 193–204) and α-helices 8 and 9 (residues 148–204) (V. M. Bolanos-Garcia and T. L. Blundell, unpublished results).

Interestingly, the crystal structure of the TPR domain of cyclophilin 40 shows an extended form, which has been attributed to a trapped folding intermediate (44). If this is the case, it means that the interactions in the crystal lattice were sufficiently strong to stabilize protein molecules in different conformational states. In the same crystal structure, it was also observed that the C-terminal region of a neighboring molecule bonds to the concave face of the characteristic superhelical structure of TPR motifs, suggesting that the binding of TPR ligands is sufficient to stabilize this fold. Moreover, recent studies on the TPR motif of PP5 unveiled a coupled ligand binding-folding mechanism (48). Besides, the coupled ligand binding-folding mechanism may be common in this class of repeat motif (48). Taken together, these findings might explain why only quite a few examples of TPR motifs have been crystallized in the absence of any ligand. Those observations may also provide an explanation of the dimeric oligomerization state often observed in the crystal structure of TPR motifs. We have obtained protein crystals of the TPR motif of human BUBR1 (residues 1–213) that were suitable for x-ray diffraction studies (i.e., single crystals 300–500 μm in size). However, the maximum diffraction limit achieved using synchrotron radiation was in the order of 6 Å even though the crystals did not decay rapidly (V. M. Bolanos-Garcia and T. L. Blundell, unpublished results). A plausible explanation for the poor diffraction limit achieved is that protein molecules exhibited diverse conformational states in the crystal lattice just as seen in the TPR motif of cyclophilin 40. From these observations, it seems either that the cocrystallization of the N-terminal domain of BUBR1 with its ligand(s) might be crucial to obtain single crystals of higher quality or that, if a stable construct of this domain can be crystallized in the absence of any ligand(s), it will form homodimers or higher-order oligomers in the crystalline state.

This work provides a new physical insight of the N-terminal region of BUBR1, a protein that plays an essential role in the mitotic checkpoint control. We have provided evidence that this region (residues 1–204) exhibits a high α-helical content, remains stable in a wide range of pH and exhibits a close similarity to the TPR motif of PP5 (residues 16–181) with respect to its secondary structure content, globularity, adsorption, and rheological properties at air/water interfaces. The presence of a putative TPR motif in the N-terminal region of BUBR1 strongly suggests that this region directly participates in protein-protein and/or protein-lipid interactions, a notion supported by the high surface activity observed at air/water interfaces. However, the direct participation of lipids in the regulation of any mitotic checkpoint protein has not been reported to date.

The putative TPR motif might in turn provide the structural framework for some of the functions of this multidomain checkpoint control protein. Undoubtedly, the identification of interacting partner(s) of the putative TPR motif of BUBR1 will give new insights into the function of BUBR1 and, at the same time, increase the chances of obtaining single crystals of high quality. Both are aspects currently being investigated in our laboratory.

We are very grateful to Dr. Michael Chinkers (University of South Alabama) for providing us with the TPR-PP5 clone, to Dr. Nuria Campillo for initial modeling studies, and to Dr. Bernard Desbat for critical review of the manuscript.

V.M.B.-G. and T.L.B. are very grateful to Cancer Research UK for financial support received (CRUK C506/A3846).

REFERENCES

1. Jallepalli, P. V., and C. Lengauer. 2001. Chromosome segregation and cancer: cutting through the mystery. *Nat. Rev. Cancer.* 1:109–117.
2. Gorbsky, G. J. 2001. The mitotic spindle checkpoint. *Curr. Biol.* 11: R1001–R1004.
3. Chan, G. K., S. A. Jablonski, V. Sudakin, J. C. Hittle, and T. J. Yen. 1999. Human BUBR1 is a mitotic checkpoint kinase that monitors CENP-E functions at kinetochores and binds the cyclosome/APC. *J. Cell Biol.* 146:941–954.
4. Rieder, C. L., A. Schultz, R. Cole, and G. Sluder. 1994. Anaphase onset in vertebrate somatic cells is controlled by a checkpoint that monitors sister kinetochore attachment to the spindle. *J. Cell Biol.* 127:1301–1310.
5. Li, X., and R. B. Nicklas. 1995. Mitotic forces control a cell-cycle checkpoint. *Nature.* 373:630–632.
6. Chan, G. K., B. T. Schaar, and T. J. Yen. 1998. Characterization of the kinetochore binding domain of CENP-E reveals interactions with the kinetochore proteins CENP-F and hBUBR1. *J. Cell Biol.* 143:49–63.
7. Tang, Z., R. Bharadwaj, B. Li, and H. Yu. 2001. Mad2-independent inhibition of APCCdc20 by the mitotic checkpoint protein BUBR1. *Dev. Cell.* 1:227–237.

8. Kitajima, T. S., S. A. Kawashima, and Y. Watanabe. 2004. The conserved kinetochore protein shugoshin protects centromeric cohesion during meiosis. *Nature*. 427:510–517.

9. Cahill, D. P., C. Lengauer, J. Yu, G. J. Riggins, J. K. Willson, S. D. Markowitz, K. W. Kinzler, and B. Vogelstein. 1998. Mutations of mitotic checkpoint genes in human cancers. *Nature*. 392:300–303.

10. Grabsch, H. I., J. M. Askham, E. E. Morrison, N. Pomjanski, K. Lickvers, W. J. Parsons, A. Boecking, H. E. Gabbert, and W. Mueller. 2004. Expression of BUB1 protein in gastric cancer correlates with the histological subtype, but not with DNA ploidy or microsatellite instability. *J. Pathol.* 202:208–214.

11. Hanks, S., K. Coleman, S. Reid, A. Plaja, H. Firth, D. Fitzpatrick, A. Kidd, K. Mehes, R. Nash, N. Robin, N. Shannon, J. Tolmie, J. Swansbury, A. Irrthum, J. Douglas, and N. Rahman. 2004. Constitutional aneuploidy and cancer predisposition caused by biallelic mutations in BUB1B. *Nat. Genet.* 36:1159–1161.

12. Millband, D. N., and K. G. Hardwick. 2002. Fission yeast Mad3p is required for Mad2p to inhibit the anaphase-promoting complex and localizes to kinetochores in a BUB1p-, Bub3p-, and Mph1p-dependent manner. *Mol. Cell. Biol.* 22:2728–2742.

13. Pfleger, C. M., and M. W. Kirschner. 2000. The KEN box: an APC recognition signal distinct from the D box targeted by Cdh1. *Genes Dev.* 14:655–665.

14. King, R. W., J. M. Peters, S. Tugendreich, M. Rolfe, P. Hieter, and M. W. Kirschner. 1995. A 20S complex containing cdc27 and cdc16 catalyses the mitosis-specific conjugation of ubiquitin to cyclin B. *Cell.* 81:279–288.

15. Lamb, J. R., S. Tugendreich, and P. Hieter. 1995. Tetratricopeptide repeat interactions: to TPR or not to TPR? *Trends Biochem. Sci.* 20:257–259.

16. Das, K. A., P. T. W. Cohen, and D. Barford. 1998. The structure of the tetratricopeptide repeats of protein phosphatase 5: implications for TPR-mediated protein-protein interactions. *EMBO J.* 17:1192–1199.

17. Zhao, S., and A. Sancar. 1997. Human blue-light photoreceptor hCRY2 specifically interacts with protein serine/threonine phosphatase 5 and modulates its activity. *Photochem. Photobiol.* 66:727–731.

18. Chinkers, M. 1994. Targeting of a distinctive protein-serine phosphatase to the protein kinase-like domain of the atrial natriuretic peptide receptor. *Proc. Natl. Acad. Sci. USA.* 91:11075–11079.

19. Kang, H., S. L. Sayner, K. L. Gross, L. C. Russell, and M. Chinkers. 2001. Identification of amino acids in the tetratricopeptide repeat and C-terminal domains of protein phosphatase 5 involved in autoinhibition and lipid activation. *Biochemistry.* 40:10485–10490.

20. Bolanos-Garcia, V. M., J. Mas-Oliva, S. Ramos, and R. Castillo. 1999. Phase transitions in monolayers of human apolipoprotein C–I. *J. Phys. Chem. B.* 103:6236–6242.

21. Chen, X., C. C. Moser, D. L. Pillud, and P. L. Dutton. 1998. Molecular orientation of Langmuir Blodgett films of designed heme protein and lipoprotein maquettes. *J. Phys. Chem. B.* 102:6424–6432.

22. Dubreil, L., V. Vie, S. Beaufils, D. Marion, and A. Renault. 2003. Aggregation of puroindoline in phospholipid monolayers spread at the air-liquid interface. *Biophys. J.* 85:2650–2660.

23. Bolanos-Garcia, V. M., and R. Nunez-Miguel. 2003. On the structure and function of apolipoproteins: more than a family of lipid-binding proteins. *Prog. Biophys. Mol. Biol.* 83:47–68.

24. Eisenberg, D., R. M. Weiss, and T. C. Terwilliger. 1982. The helical hydrophobic moment: a measure of the amphiphilicity of a helix. *Nature.* 299:371–374.

25. Shi, J., T. L. Blundell, and K. Mizuguchi. 2001. FUGUE: sequence-structure homology recognition using environment-specific substitution tables and structure-dependent gap penalties. *J. Mol. Biol.* 310:243–257.

26. Brewerton, S. 2004. Structural annotation of protein sequences: tools for construct design. PhD thesis. University of Cambridge, England.

27. Sali, A., and T. L. Blundell. 1993. Comparative protein modelling by satisfaction of spatial restraints. *J. Mol. Biol.* 234:779–815.

28. Sreerama, N., and R. W. Woody. 2000. Estimation of protein secondary structure from CD spectra: Comparison of CONTIN, SELCON and CDSSTR methods with an expanded reference set. *Anal. Biochem.* 282:252–260.

29. Bolanos-Garcia, V. M., M. Soriano-Garcia, and J. Mas-Oliva. 1998. Stability of the C-terminal peptide of CETP mediated through an (i, i + 4) array. *Biochim. Biophys. Acta.* 1384:7–15.

30. Svergun, D. I. 1991. Mathematical methods in small-angle scattering data analysis. *J. Appl. Crystallogr.* 24:485–492.

31. Berge, B., and A. Renault. 1993. Ellipsometry study of 2D crystallization of 1-alcohol monolayers at the water surface. *Europhys. Lett.* 21: 773–777.

32. Azzam, R. M. A., and N. M. Bashara. 1977. Ellipsomety and Polarized Light, North Holland, Amsterdam. 340.

33. De Feijter, J. A., J. Benjamins, and F. A. Veer. 1978. Ellipsometry as a tool to study the adsorption behavior of synthetic and biopolymers at the air-water interface. *Biopolymers.* 17:1759–1772.

34. Venien-Bryan, C., P.-F. Lenne, C. Zakri, A. Renault, A. Brisson, J.-F. Legrand, and B. Berge. 1998. Characterization of the growth of 2D protein crystal on a lipid monolayer by ellipsometry and rigidity measurements coupled to electron microscopy. *Biophys. J.* 74:2649–2657.

35. Renault, A., P.-F. Lenne, C. Zakri, A. Aradian, C. Venien-Bryan, and F. Amblard. 1999. Surface-induced polymerization of actin. *Biophys. J.* 76:1580–1590.

36. Main, E. R. G., Y. Xiong, M. J. Cocco, L. D'Andrea, and L. Regan. 2003. Design of stable alpha-helical arrays from an idealized TPR motif. *Structure.* 11:497–508.

37. Bolanos-Garcia, V. M., S. Ramos, R. Castillo, J. Xicohtencatl-Cortes, and J. Mas-Oliva. 2001. Monolayers of apolipoproteins at the air/water interface. *J. Phys. Chem. B.* 105:5757–5765.

38. Krebs, K. E., and M. C. Phillips. 1984. The contribution of alpha-helices to the surface activities of proteins. *FEBS Lett.* 175:263–266.

39. Krebs, K. E., and M. C. Phillips. 1983. The helical hydrophobic moments and surface activities of serum apolipoproteins. *Biochim. Biophys. Acta.* 754:227–230.

40. Damodaran, S., and C. S. Rao. 2001. Molecular basis for protein adsorption at fluid-fluid interfaces. *In* Food Colloids: Fundamentals of Formulation. E. Dickinson and R. Miller, editors. Royal Society of Chemistry, London. 165–180.

41. Ward, A. F., and L. Tordai. 1946. Time dependence of boundary tensions of solutions. I. The role of diffusion in the time effects. *J. Chem. Phys.* 14:453–461.

42. D'Andrea, L., and L. Regan. 2003. TPR proteins: the versatile helix. *Trends Biochem. Sci.* 28:655–662.

43. Scheufler, C., A. Brinker, G. Bourenkov, S. Pegoraro, L. Moroder, H. Bartunik, F. U. Hartl, and I. Moarefi. 2000. Structure of TPR domain-peptide complexes: critical elements in the assembly of the Hsp70-Hsp90 multichaperone machine. *Cell.* 101:199–210.

44. Taylor, P., J. Dornan, A. Carrello, R. F. Minchin, T. Ratajczak, and M. D. Walkinshaw. 2001. Two structures of cyclophilin 40: folding and fidelity in the TPR domains. *Structure.* 9:431–438.

45. Wilson, C. G., T. Kajander, and L. Regan. 2005. The crystal structure of NlpI. A prokaryotic tetratricopeptide repeat protein with a globular fold. *FEBS J.* 272:166–179.

46. Fröberg, J. C., T. Arnebrant, J. McGuire, and P. M. Claesson. 1998. Effect of structural stability on the characteristics of adsorbed layers of T4 lysozyme. *Langmuir.* 14:456–462.

47. Gromiha, M. M., and S. Selvaraj. 2004. Inter-residue interactions in protein folding and stability. *Prog. Biophys. Mol. Biol.* 86:235–277.

48. Cliff, M. J., M. A. Williams, J. Brooke-Smith, D. Barford, and J. E. Ladbury. 2005. Molecular recognition via coupled folding and binding in a TPR domain. *J. Mol. Biol.* 346:717–732.